EFFECTS OF HOUSING GEOMETRY ON THE PERFORMANCE AND NOISE OF A TWO-OUTLET CENTRIFUGAL FAN – A NUMERICAL STUDY

Ian Yin Wai WONG[1], Randolph Chi Kin LEUNG[1],
Anthony Kwok Yung LAW[2]

[1] *Department of Mechanical Engineering, The Hong Kong Polytechnic University, Hung Hom, Kowloon, Hong Kong, P. R. China*

[2] *Raymond Industrial Limited, 18/F, Grandtech Centre, 8 On Ping Street, New Territoties, Hong Kong, P. R. China*

SUMMARY

A two-outlet centrifugal fan design aiming at providing high mass flow rate but low noise level was investigated. The analysis was carried out using computational fluid dynamics (CFD) software (Fluent 6.3). Two dimensional unsteady flow simulation on existing fan was done. A three dimensional simulation was then carried out to compare the results with the two dimensional one; the key flow dynamics and key fan performance parameters calculated were consistent between the two simulations. As a result, in order to save time and effort, two dimensional simulations were carried out to analyze the effects of the ratio between cutoff distance and the radius of curvature of the fan housing to the fan flow dynamics and its subsequent noise radiation. One of the designs proposed was able to deliver a mass flow rate 34% more but with 10dB lower sound pressure level. This founding was verified by testing at the manufacturer laboratory.

INTRODUCTION

It is common that many domestic products containing centrifugal fans are very noisy. The flow through a centrifugal fan is unsteady and highly three dimensional; thus, traditional fan design approach based on trial and error are no longer possible. Nowadays, it is necessary to determine the sources of noise from this centrifugal fan in a fast and low cost manner so as to give shorter design cycles. Thus in fan industry, the use of Computational fluid dynamics (CFD) is getting popular for identifying the fan noise generation mechanisms.

Many researchers have attempted to investigate the noise generation of centrifugal fan. They found that the level of noise is associated with the degree of unsteadiness of the flow between fan blades and fan volute [1-6]. Noise reduction design modifications were proposed by some of these researchers. However, most of the proposed methods would degrade the fan performances as the

suggested modifications usually offset the best efficiency point of the fan. Therefore, these proposed low-noise designs are contradictory to those favoring high mass flow rate requirements.

In this paper, the dynamics of flow through a novel centrifugal fan design, which contains two outlets, was analyzed using a commercial CFD code, Fluent 6.3. This two-outlet centrifugal fan is designed for domestic air purifier application in which a low noise radiation is a strict custom requirement. Two dimensional (2D) and three dimensional (3D) simulations were performed. The 2D simulation results of the existing fan were validated by the mass flow rate measurement and found consistent with the 3D one. Thus, 2D simulations were adopted for the proposed designs in this study in order to save computational cost and time. Based on the CFD results, the capability of fan noise radiation is evaluated using the Ffowcs Williams and Hawkings (FW-H) equation. The objective of the present work is to study the effects of fan geometrical parameters on the fan flow unsteadiness and noise generation with an aim to find out an optimal design which gives higher mass flow rate but lower noise than the existing design.

FORMULATION OF NUMERICAL PROBLEM

Numerical simulations of two-outlet industrial centrifugal fan with existing and new designs are carried out. Key fan parameters for existing fan are given in Table 1. A schematic sketch of the fan design is illustrated in Figure 1.

Table 1: Key fan parameters

Impeller		**Fan Housing**	
Blade number	50 (forward curved)	**Inlet diameter**	150 mm
Blade thickness	1.6 mm	**Outlet size**	110×65 mm
Blade chord length	38 mm	**Volute shape**	Logarithmic profile
Inlet blade angle	30º		
Outlet blade angle	75º		
Impeller inlet diameter	170 mm		
Impeller outlet diameter	245 mm		
Rotational speed	1000 rpm		

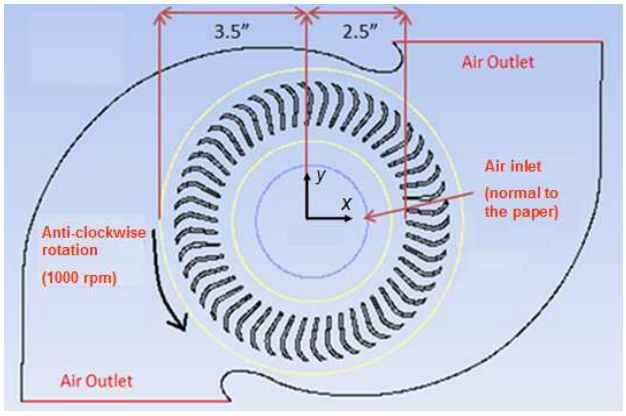

(a)

Figure 1: (a) Schematic sketch of the fan.

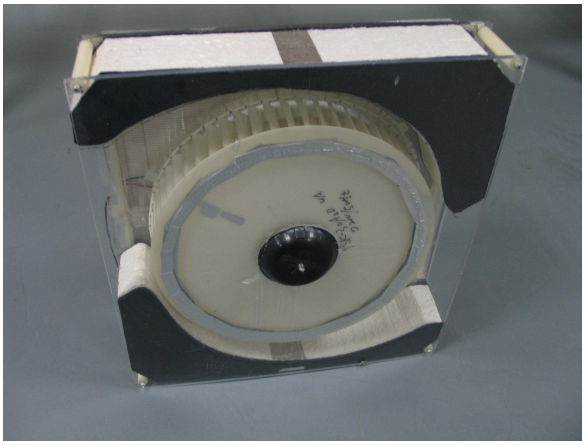

(b)

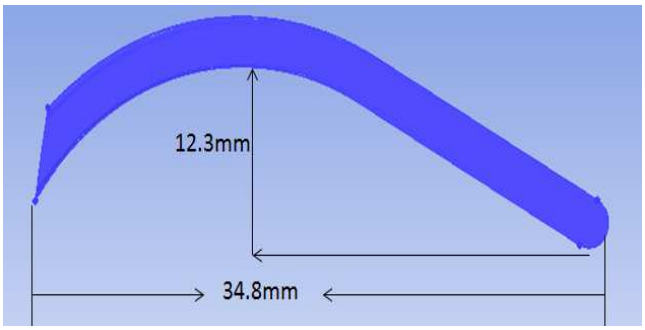

(c)

Figure 1: (b) engineering prototype of existing fan and (c) the blade geometry.

As mentioned, both 2D and 3D simulations were performed for this two-outlet centrifugal fan. The 2D simulation was compared with the 3D one which aimed to see if the flow dynamics is dominated by 2D features. In both simulations, the computational domains were divided into two zones, a rotating zone including the impeller and a stationary zone elsewhere. The sliding mesh technique was applied to the interfaces in order to allow the unsteady interactions between the two zones. In the two sets of simulations, two different numerical approaches were applied. They are the unsteady Reynolds averaged Navier-Stokes (URANS) approach and Large eddy simulation (LES). URANS approach could shorten the computational effort and time but has its limitations for resolving small scale eddies. This is because Reynolds averaging is a simplification that loses the information contained in the full Navier-Stokes equation. However, for fan with low Mach number flow speed, as presented in this paper, URANS approach could give a good prediction of the fan performances [2]. Therefore, in the 2D simulation, URANS was applied which aimed to simulate the dynamics of the fan flow in the fastest way and provide good enough data for the manufacturer to evaluate the fan performances.

On the other hand, LES, computes the large eddies directly and the small, "subgrid-scale" eddies are modeled. The underlying premise is that the large eddies are directly affected by the boundary conditions, carry most of the Reynolds stress and thus are computed. The small-scale turbulence is weaker; contributing less to the Reynolds stresses and so is more amenable to modeling. Therefore, LES is a more promising mode of numerical simulation of turbulence but it also requires a much higher computational cost and time than the URANS does. LES was applied in the 3D simulation so that its results could be used to assess the capability of the 2D simulation by comparing the key flow features. The numerical setup of the 2D and 3D simulations are summarized in Table 2.

2D simulation

Two-dimensional URANS simulation of the centrifugal fan flow was carried out using finite volume method on an unstructured mesh generated within the computational domain illustrated in Figure 1. The second-order, implicit segregated solver available in Fluent 6.3 with SIMPLE algorithm [7] for pressure-velocity coupling was used. Standard $k-\varepsilon$ model with 5% turbulence intensity was adopted to account for the turbulence effects. Enhanced wall modeling was applied which combined a two-layer model with enhanced wall function. In the two-layer model [9], the whole domain was divided into a viscosity affected region and a fully turbulent region. The enhanced wall function extended the applicability throughout the near-wall region by formulating the law-of-wall as a single wall law for the entire wall region. This was achieved by blending linear and logarithmic laws-of-wall using a function suggested by Kader [10]. Pressure inlet and pressure

outlet boundary conditions with standard atmosphere pressure were set at fan inlet and outlet. No-slip boundary conditions were used on all solid surfaces. Implicit scheme was used for time-marching so there was no stability criterion to be met in determining the time step size. However, in order to model transient phenomena correctly, the time step size should be properly determined. For explicit scheme, it requires the CFL<1. This condition was also applied here, the time step size of the calculation was eventually set to 2×10^{-4} sec. so that the solution in each time step could converge within 10 iterations. This could greatly save the computational time. The same approach for determining the time step size was applied to the 3D simulation.

3D simulation

LES with wall adapting local eddy viscosity (WALE) sub-grid scale model was applied in 3D simulation. The governing equations employed for LES are obtained by filtering the time-dependent incompressible Navier-Stokes equations. The filtering process effectively filters out the eddies with scales smaller than the filter width. This filtering operation results a stress tensor called "subgrid-scale stress tensor" which is an unknown that needs to be modeled. WALE model proposed by Ducros [11] was used which was designed to recover the correct asymptotic behaviour of the subgrid viscosity at the wall in zero-pressure gradient incompressible boundary layers and account for wall damping effects without using a damping function. The second-order, implicit segregated solver with SIMPLE algorithm [7] for pressure-velocity coupling was used. Second order, bounded central differencing scheme was used for convection and diffusion terms. No-slip boundary conditions were used on all solid surfaces. The time step size of the calculations was set to 5×10^{-6} sec.

Table 2: Summary of numerical setup and the distribution of grid numbers

Numerical setup		
	2D	**3D**
Turbulence modeling	*k-ε* model (URANS approach)	LES (WALE as subgrid scale model)
Time dependent scheme	Second order, implicit	Second order, implicit
Pressure-velocity coupling	SIMPLE algorithm	SIMPLE algorithm
Solid surface	No-slip	No-slip
Inlet	Pressure inlet	Pressure inlet
Outlet	Pressure outlet	Pressure outlet
Time step size	2×10^{-4} sec	5×10^{-6} sec
Distribution of grid numbers		
Inlet (upstream extent)	25614	829552
Impeller (rotational zone)	58672	1514490
Fan housing	86245	1513415

VALIDATION OF NUMERICAL SIMULATIONS

Every numerical simulation needs be validated by experiment before the results can be used for further evaluations. The simulations done in the present paper was validated by comparing the calculated mass flow rate to the measured one. The mass flow rates ($\dot{m}$) calculated from numerical simulations at time-stationary state (5 revolution's time, about 0.3 sec.) and measured from experiment are given in Table 3. The differences between 2D simulation, 3D simulation and measurement were small (within 4% of deviation). For the flow rate measurement, as shown in Figure 2 (the test unit is given in Figure 1b), the Velocicalc air velocity meter was used for measuring the air flow. The fan outlets were divided into ten equal units. The air velocity meter measured the flow speed at each center point of the unit and this is the mean flow speed of that unit. The mass flow rate is thus found by multiplying the unit mean flow speeds (V_i) to the unit areas (A_i), i.e. $\dot{m} = \rho \int_A V dA \approx \rho \sum V_i A_i$.

(a) (b)

Figure 2: Flow rate measurement: (a) Air flow meter and (b) Cross section of fan outlet measuring surface.

Table 3: Mass flow rate comparison

	Mass flow rate (CFM)	**Difference from measurement**
2D simulation	204.37	2.19%
3D simulation	197.16	1.42%
Measurement	200	/

SIMULATION RESULTS OF EXISTING DESIGN

Figures 3 shows the vorticity distributions obtained from 2D and 3D simulations. The scaling of the magnitude of the properties are the same in the two figures. In 3D simulation, data was taken an imaginary plane passing through the midspan of all blades. In the Figure, it can be seen that high vorticity region are found in the impeller region in both 2D and 3D simulation. According to the results obtained from the 3D simulation, the vortex moving along the blade, from leading edge to the trailing edge and continue growing to interact with the fan housing. Eventually, the vortex interacts with the volute tongue and creates strong flow unsteadiness at that region. The magnitude of the vortex in 2D simulation was also highest within the impeller, much higher than that in the other region of the fan, which was consistent with the 3D one. These results showed that the noise

sources in the impeller region are stronger according to the FW-H theory. However, the movement of the vortex was not clearly uncovered in the 2D simulation, it only showed the vorticity was highest at the blade trailing edge near the volute tongue region. This difference accounted the deficiency of 2D simulation with URANS approach in which the small scale eddies was limitedly calculated.

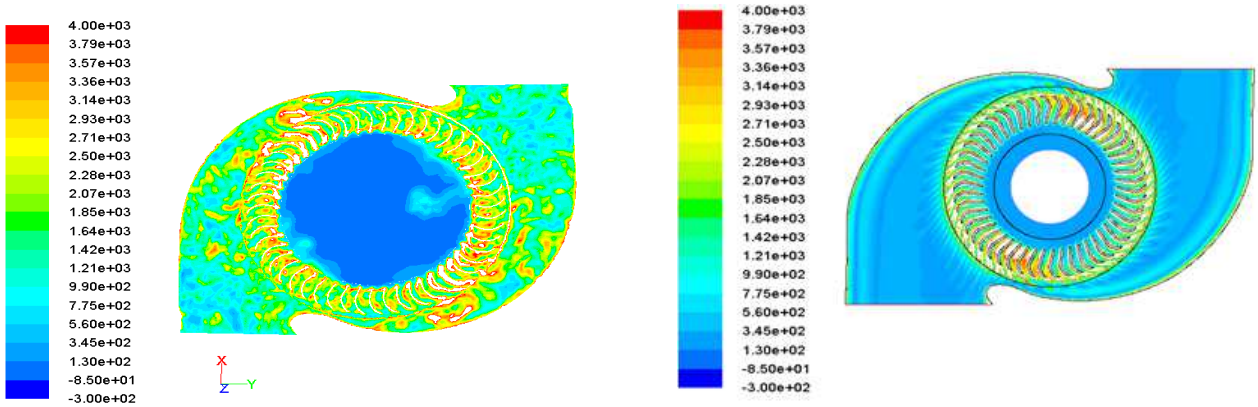

(a) (b)

Figure 3: Contour of vorticity at time interval=0.3 second (anticlockwise rotation): (a) 3D simulation; (b) 2D simulation.

Aeroacoustics of 2D and 3D simulations

Ffowcs Williams and Hawkings Equation [8] is the extension of the Lighthill's acoustics analogy [12] which includes the influence of arbitrarily moving surfaces. FW-H equation is generalized as:

$$\frac{\partial^2 \rho'}{\partial t^2} - c_0^2 \frac{\partial^2 \rho'}{\partial x_i^2} = \frac{\partial^2 T_{ij}}{\partial x_i \partial x_j} - \frac{\partial}{\partial x_i}\left(p_{ij}\delta(f)\frac{\partial f}{\partial x_j}\right) + \frac{\partial}{\partial t}\left(\rho_0 u_i \delta(f)\frac{\partial f}{\partial x_i}\right). \quad (1)$$

The first term on the right hand side of Equation 2 is the quadrupole term which is associated with the flow turbulence. Its strength is given by the Lighthill tensor T_{ij}. The second term is the dipole term. It is proportional to the stress tensor p_{ij} which contains the viscous stresses and the aerodynamic pressure. The dipole strength is given by the force vector which acts from the surface onto the fluid. The third term is the monopole term which is related to the blade thickness, the displacement volume of the blade. In this work, the monopole and quadrupole term were not taken into account as the blade thickness are very thin and the flow Mach number of the fan is low. The solutions of the FW-H equation were obtained from the free field green function. The effects of wave reflection and scattering due to the presence of the fan housing were neglected. Therefore, in the present paper, FW-H equation was only used to assess the noise generation capability at the source. To achieve this, compact noise radiation was assumed as the impeller diameter (0.245m) is much smaller than the shortest wavelength of interest (1.7m). In general, for the contributions of n noise sources, the acoustic pressure of loading noise was obtained by the formulas given by Succi [13] and Farassat [14]

$$p(\vec{x},t) = \sum_{i=1}^{n_s} p_{\ln,i}(t) + p_{lf,i}(t). \quad (2)$$

The two terms represent the effect of impeller loading in the near field $p_{\ln,i}(t)$, which is,

$$p_{\ln,i}(t)=\frac{1}{4\pi}\left[\frac{1}{(1-M_r)^2 r^2}\left(\vec{r}_i\cdot\vec{f}_i\frac{1-\vec{M}_i\cdot\vec{M}_i}{1-M_r}-\vec{f}_i\cdot\vec{M}_i\right)\right]_{ret}, \tag{3}$$

and the far field $p_{lf,i}(t)$ given by

$$p_{lf,i}(t)=\frac{1}{4\pi}\left[\frac{1}{(1-M_r)^2 r^2}\left(\frac{\vec{r}_i}{c_0}\frac{\partial\vec{f}_i}{\partial t}+\frac{\vec{r}_i\cdot\vec{f}_i}{1-M_r}\left(\frac{\vec{r}_i}{c_0}\cdot\frac{\partial\vec{M}_i}{\partial t}\right)\right)\right]_{ret}. \tag{4}$$

The impeller loading accounts for the noise generated by the forces acting on the fluid. The main parameters affecting the noise as written in the formulas are the source Mach vector, $\vec{M}_i=(1/c_0)(\partial\vec{y}/\partial t)$, its first time derivative, $(\partial\vec{M}_i/\partial t)=(1/c_0)(\partial^2\vec{y}_i/\partial t^2)$ and the relative Mach number, $M_r=(\vec{x}_i-\vec{y}_i/r)\cdot(1/c_0)(\partial\vec{y}_i/\partial t)=\vec{r}_i\cdot\vec{M}_i$. The terms in the square brackets of Equations 3 and 4 are evaluated at retarded time. In the equations, c_0 is the speed of sound, $\vec{r}_i$ is a unit vector from the noise source *i* to the observer and f_i is the force vector acting onto the fluid. In the present work, as the noise source is assumed compact and the impeller is rotating at a constant speed, simplifications could be done to Equations 3 and 4. The Mach vector $\vec{M}_i$ is equal to constant, M_i is approximately equal to constant *M* and r_i is approximately equal to constant *r*. Thus, $\partial\vec{M}_i/\partial t$ is equal to zero and M_r is a constant. These two equations are therefore simplified as

$$p_{\ln,i}(t)=c_1\sum\nolimits_i^n\vec{f}_i(t)=c_1\sum\nolimits_i^n\vec{C}_i(t) \tag{5}$$

and

$$p_{lf,i}(t)=c_2\frac{\partial\sum_i^n\vec{f}(t)_i}{\partial t}=c_2\frac{\partial\sum_i^n\vec{C}_i(t)}{\partial t}. \tag{6}$$

The total acoustic pressure of loading noise is approximated as

$$p(\vec{x},t)\approx c_1\vec{C}(t)+c_2\frac{\partial\vec{C}(t)}{\partial t}, \tag{7}$$

where $c_1=(1/4\pi)\left[\left(1/(1-M_r)^2 r^2\right)-\left(\left((1-M^2)r/1-M_r\right)-M\right)\right]$ and $c_2=(1/4\pi)\left[\left(1/(1-M_r)^2 r^2\right)(r/c_0)\right]$ respectively. $\vec{C}(t)$ can be seen as the overall force coefficients, i.e. the vector sum of drag $\vec{C}_D(t)$ and lift $\vec{C}_L(t)$ coefficients of impeller. That is

$$\vec{C}(t)=C_L(t)\hat{i}+C_D(t)\hat{j}, \tag{8}$$

and the time derivative is,

$$\frac{\partial\vec{C}(t)}{\partial t}=\frac{\partial C_L(t)}{\partial t}\hat{i}+\frac{\partial C_D(t)}{\partial t}\hat{j}. \tag{9}$$

The change in *SPL* was estimated by

$$\Delta SPL=10\log_{10}\frac{\left|c_1\vec{C}(t)+c_2\frac{\partial\vec{C}(t)}{\partial t}\right|^2}{\left|c_1\vec{C}_{existing}(t)+c_2\frac{\partial\vec{C}_{existing}(t)}{\partial t}\right|^2}. \tag{10}$$

Figure 4 shows a comparison of the spectra obtained from the results of 2D and 3D simulations. Both show a peak at 33.33Hz which is the double of the impeller rotation frequency. However, in the third harmonic, the magnitude of the power spectrum density obtained from 2D was obviously lower than that of 3D. The overall magnitude was also smaller in 2D, this is due to its limitation of calculating the vortices which is highly three dimensional and thus the calculated level of interaction between flowing fluid and impeller was lower.

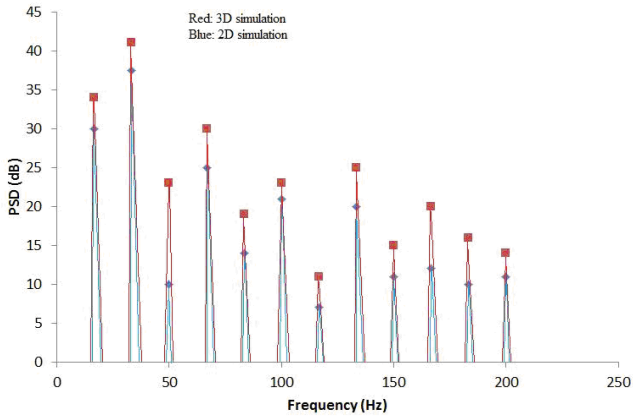

Figure 4: Spectrum of overall force coefficients $\vec{C}(t)$. 2D: blue line; 3D: red line.

The same pattern of the power spectrum density between 2D and 3D simulations can be explained by the time variation of $\vec{C}_L(t)$ and $\vec{C}_D(t)$ as well as its time derivative $d\vec{C}_L(t)/dt$ and $d\vec{C}_D(t)/dt$ as shown in Figure 5. The variation patterns of the coefficients between these two simulations are consistent with differences in the magnitude.

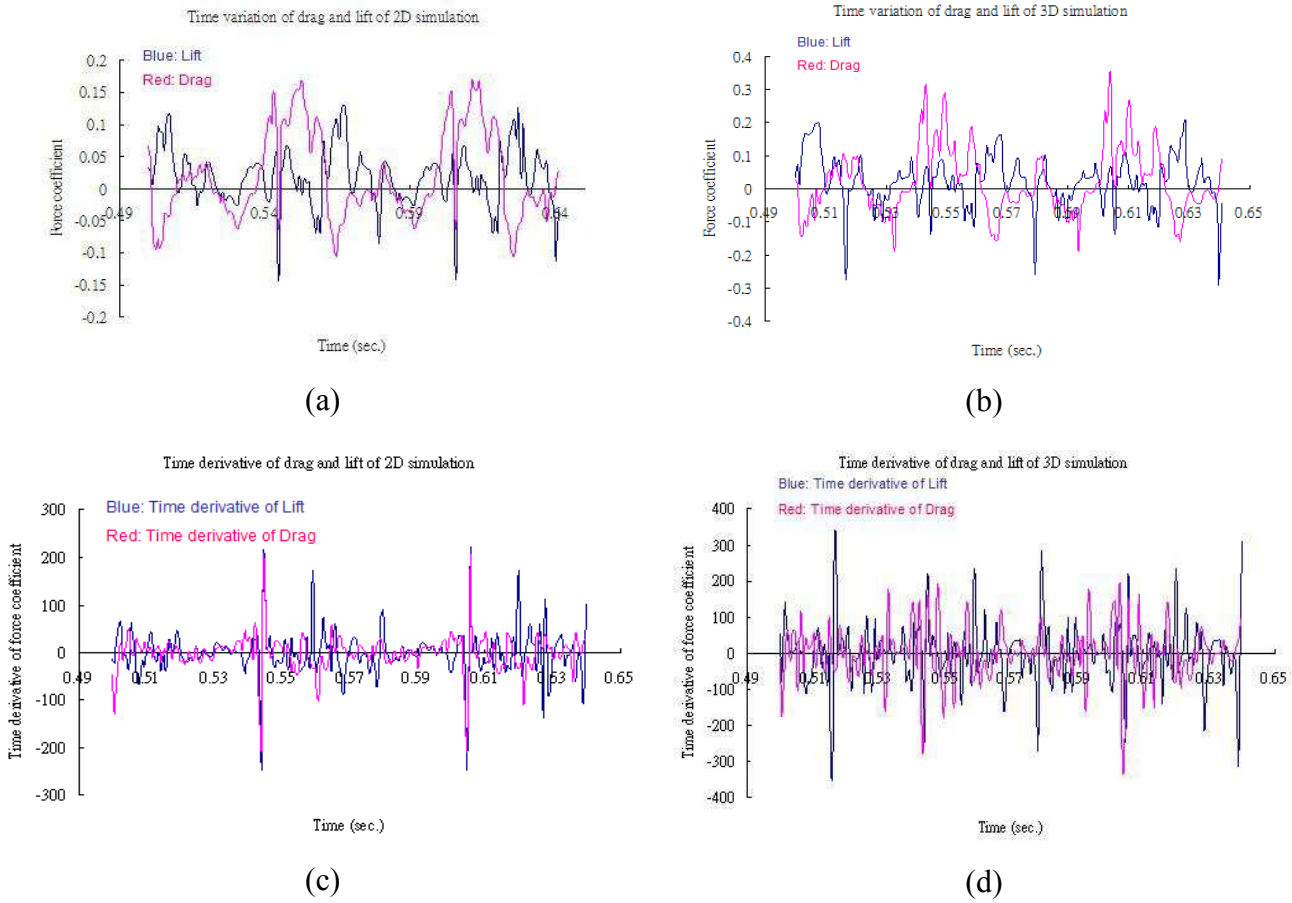

Figure 5: Time variation of (2 cycles' time): (a) $C_L(t)$and $C_D(t)$ of 2D simulation, (b) $C_L(t)$and $C_D(t)$ of 3D simulation, (c) $dC_L(t)/dt$ and $dC_D(t)/dt$ of 2D simulation; (d) $dC_L(t)/dt$ and $dC_D(t)/dt$ of 3D simulation.

From the above results, key flow dynamics and key fan performance parameters calculated in 2D simulation were consistent with the 3D simulation. Based on these results, in order to reduce the simulation time and cost, the calculations afterwards were carried by 2D simulations which aimed to provide an insight in the dominant noise source mechanisms of the two-outlet centrifugal fan and an indication of the variation of noise level with key fan geometrical parameters. This could provide enough informative data for the fan designers to evaluate the fan designs in the fastest and lowest cost manner. The fan manufacturers thus can be benefited by the advantages of 2D simulation at fan design stage.

NEW HOUSING GEOMETRY DESIGN

After the calculations of the existing fan, four new housing designs were proposed to carry out simulations. The impeller configurations are same as the existing fan so that the noise radiation due to various housing geometries can be assessed. The new design are specified by the fan housing curvature *P* and the ratio between fan cutoff distance *m* separating fan housing volute tongue and impeller, and blade spacing *n* (Figure 6). Their combinations are listed in Table 4b. In this paper, it is reminded that the volute tongue shape was also modified in the new designs. However, the impact due to this modification was not significant compare with the fan curvature *P* and cut-off distance. This information was given from the fan manufacturer in which they have done a testing to verify the performance and noise level were not sensitive to this change. The results given by the manufacturer in this test are shown in Table 4a. Therefore, for the new designs, in order to simplify the drawings, the modified tongue shape was used in the simulations.

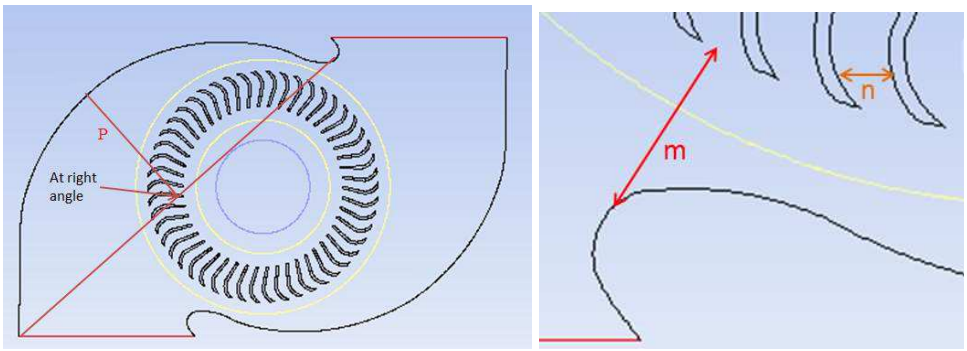

Figure 6: Definition of fan geometrical parameters P, m and n.

Table 4a: Results of modified volute tongue shape test given by manufacturer

Design	**Mass flow rate**	***SPL***
Existing	204.37 cfm	48 dB
Modified tongue shape (all others parameters are unchanged)	202.46 cfm	48.5 dB

Table 4b: Combinations of the fan designs

Design	***m : n***	***P (m)***
Existing	1 : 0.8	0.09961
1	1 : 2	0.1134
2	1 : 0.5	0.1132
3	1 : 2	0.09015
4	1 : 0.5	0.09077

RESULTS AND DISCUSSIONS

Among the four new housing designs, Design 2 gave a more desired effect of changing the geometrical parameters. The time stationary static pressure distribution for existing and Design 2 are illustrated in Figure 7. It can be seen that there exist high static pressure regions in the tip regions of the volute tongues. The pressure magnitude appears to be insensitive to the design change. Similar patterns can also be observed in other new designs. Figure 8 shows the time stationary vorticity distribution for Design 2. High vorticity regions were found around the blades and volute tongues which show that the noise sources in these regions were stronger according to FW-H theory.

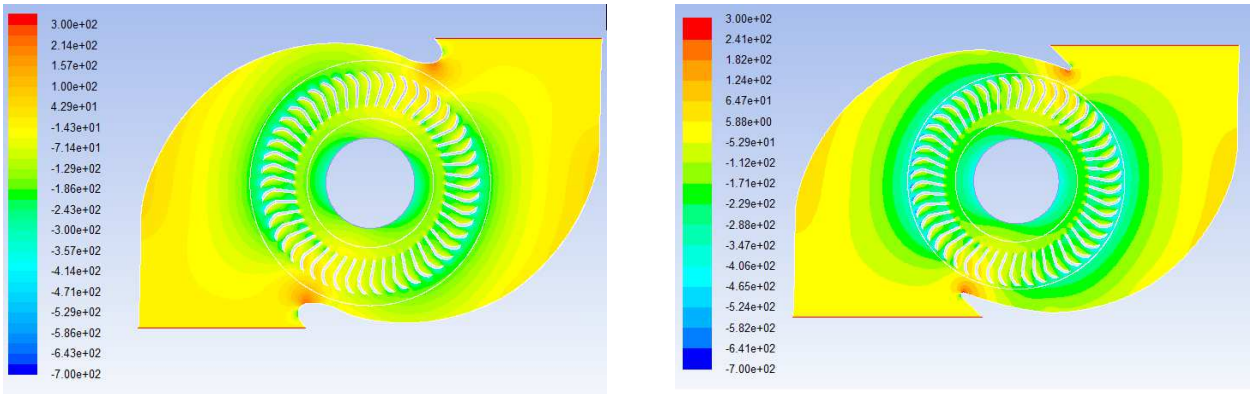

(a) (b)

Figure 7: The time stationary static pressure distribution of (a) existing design and (b) Design 2.

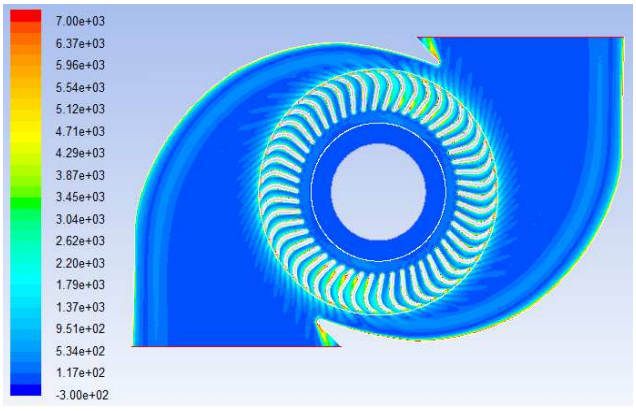

Figure 8: The time stationary vorticity distribution of Design 2.

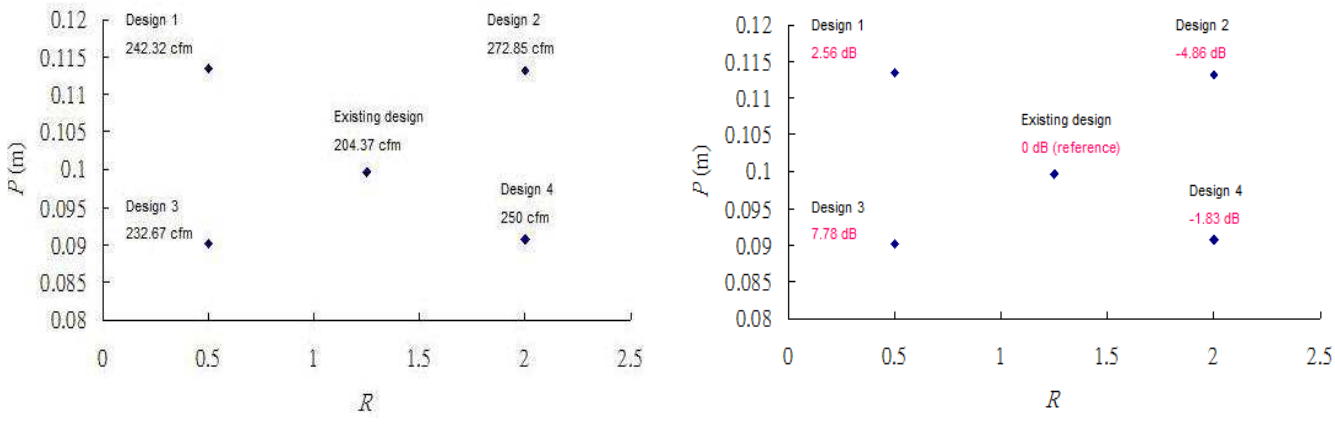

(a) (b)

Figure 9: (a)Variation of mass flow rate with P and R and (b) variation of ΔSPL with P and R.

The calculated mass flow rates of all designs are illustrated in Figure 9a. Here $R = m/n$ with n fixed. Obviously Design 2 attained maximum increase in flow rate (~34% more). This may be due to the fact that a larger cutoff distance reduced the recirculation of the flow which essentially reduced the flow blocking in the fan. From Figure 10a, the recirculation zone was clearly observed in the volute tongue region. The zone also extended and interacted with the rotating impeller blades so the flow blocking was strong there. In Design 2, the tongue geometry was so modified that the flow was more streamlined and easier to leave the outlet (Figure 10b). The flow blocking more or less disappeared and resulted in a higher average outlet velocity and a higher mass flow rate.

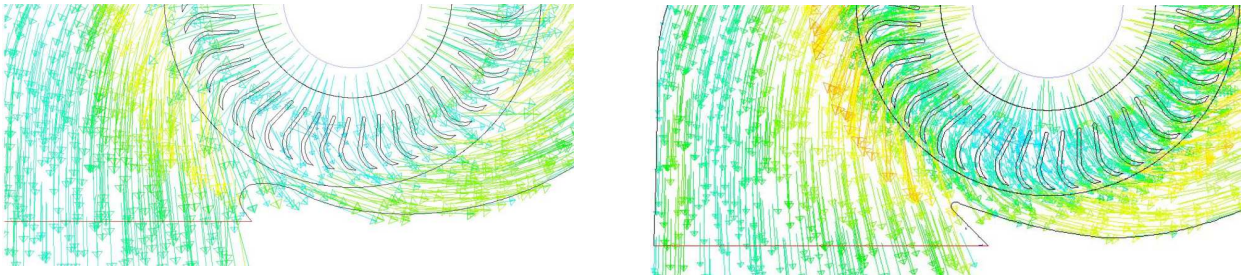

(a) (b)

Figure 10: Velocity distribution at outlet of (a) existing design and (b) design 2.

Figure 11 shows a comparison of the spectra of new and existing designs. As mentioned, only the capability of fan noise radiation was assessed here by simplifying the solutions of FW-H equation. The effect of housing geometry on flow propagation was not considered. It can be observed that the existing dominant $\vec{C}(t)$ fluctuation occurs at 33.33Hz which is equal to double of impeller rotation frequency. The double was simply due to the presence of two volute tongues. In the new designs, the dominant fluctuation however shifts to follow the impeller rotation frequency, i.e. 16.67Hz whereas other peaks were almost at the same levels as in existing design. Figure 9b shows the difference in *SPL (ΔSPL)* obtained in all new designs. It can be seen that maximum reduction of 4.86 dB was obtained from Design 2. Other designs give zero or an increase in *SPL*. Based on this result, a fan prototype of Design 2 was fabricated and tested in anechoic chamber. It was found that a 10 dB was recorded at 1m away from the fan which provides a piece of good evidence of the correctness of numerical prediction.

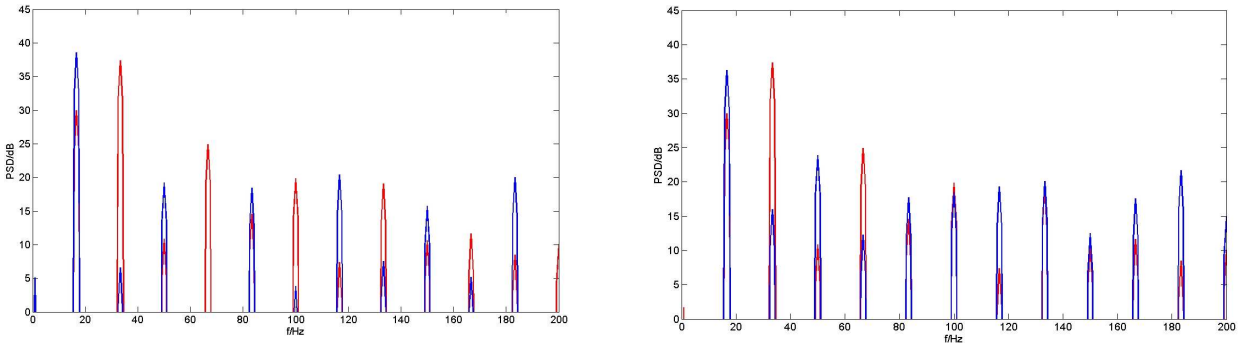

(a) Design 1 (b) Design 2

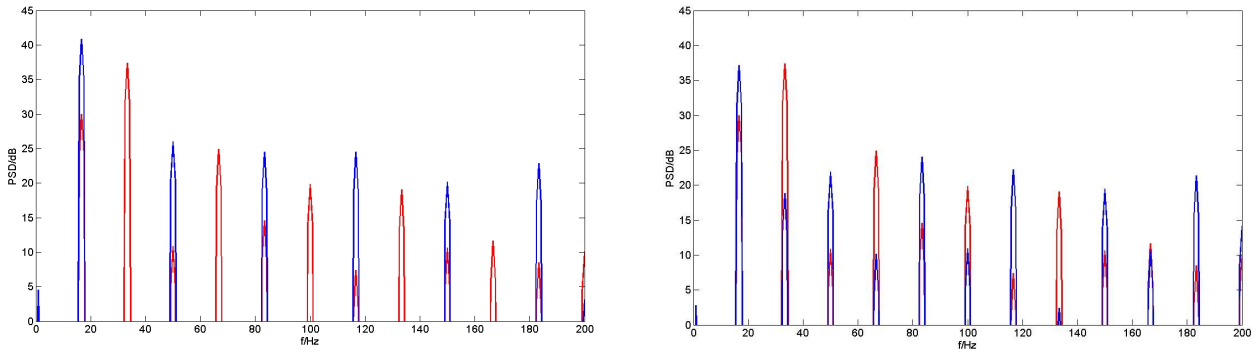

(c) Design 3 (d) Design 4

Figure 11: Spectra of overall force coefficients. Existing design: red line; new design: blue line.

CONCLUSIONS

In this paper, a numerical study of flow dynamics and aeroacoustics of an industrial centrifugal fan with two outlets is reported. Both two dimensional and three dimensional simulations were carried out for the existing fan design. In 2D simulations, the flow dynamics was calculated using URANS while LES is adopted in 3D simulation on finite volume method available from commercial CFD code and its aeroacoustic consequence was predicted using the source terms in FW-H equation. Since all key flow dynamics and key fan performance parameters calculated from 2D and 3D simulation were consistent, the two dimensional simulations were taken for further evaluation of aeroacoustics due to fan housing design changes. Analyses with existing and four new fan designs, specified with fan housing curvature and the cutoff distance at volute tongue, were carried out. Finally, Design 2, with housing profile and housing distance was found able to increase the mass flow rate and reduce *SPL*. The result was also confirmed with experiments.

ACKNOWLEDGEMENTS

The support given by University Industry Collaboration Programme, Innovation and Technology Fund of the Government of Hong Kong SAR Government under Grant Number UIT/106 is gratefully acknowledged.

Nomenclature

c_o: speed of sound

f_i: force vector acting onto the fluid

M: Mach number

M_i: local source Mach number vector

M_r: relative Mach number

r_i: modulus of $\vec{r}_i$

$\vec{r}_i$: unit vector from the noise source i to the observer

u_i: velocity component in direction i

y_i: position vector of the noise source i

ρ_0: density of the undisturbed medium

REFERENCES

[1] W.H. Jeon – *A numerical study on the effects of design parameters on the performance and noise of a centrifugal fan*. J. Sound Vib., 265: 221-230, **2003**.

[2] M. Younsi, F. Bakir – *3D unsteady flow in a centrifugal fan: impeller-volute interaction*. J. Comput. Appl. Mech., 8: 211-223, **2007**.

[3] Q. Liu, D. Qi, H. Tang – *Numerical calculation of centrifugal fan noise*. J. Mechanical Engg. Sci., 220: 1167-1177, **2007**.

[4] Q. Liu, D. Qi, H. Tang – *Computation of aerodynamic noise of centrifugal fan using large eddy simulation approach, acoustic analogy, and vortex sound theory*. J. Mechanical Engg. Sci., 221: 1132-1332, **2007**.

[5] R. B. Tajadura, S. V. Suarez, J. P. H. Cruz – *Noise prediction of a centrifugal fan: numerical results and experimental validation*. J. Fluid Engg., 130: 091102, **2008**.

[6] S. V. Suarez, R. B. Tajadura, C. S. Morros, B. P. Garcia – *Reduction of the aerodynamic tonal noise of a forward-curved centrifugal fan by modification of the volute tongue geometry*. Appl. Acoust., 69: 225-232, **2008**.

[7] J. H. Ferziger – *Computational methods for fluid dynamics*. New York: Springer-Verlag, **1996**.

[8] J. E. Ffowcs Williams, D. L. Hawkings – *Sound generation by turbulence and surfaces in arbitrary motion*. Phil. Trans. Ryo. Soc., A264, **1969**.

[9] T. Jongen – *Simulation and Modeling of Turbulent Incompressible Flows*. PhD thesis, EPD Lausanne, Lausanne, Switzerland, **1992**.

[10] B. Kader – *Temperature and Concentration Profiles in Fully Turbulent Boundary Layers.* Int. J. Heat Mass Transfer, 24: 1541-1544, **1993**.

[11] F. Ducros – *Wall-Adapting Local Eddy Viscosity Models for Simulation in Comples Geometries*. In Proceedings Conference on Numerical Methods Fluis Dynamics, Oxford, UK, **1998**.

[12] M.J. Lighthill – *On Sound Generated Aerodynamically I. General Theory*. Proceedings of the Royal Society of London, Series A, Vol 211, 564-587, **1952**.

[13] G.P. Succi – *Design of Quiet Efficient Propellers*. SAE 790584, Business Aircraft Meeting and Exposition, 1-14, **1979**.

[14] F. Farassat – *Theory of Noise Generation from Moving Bodies with an Application to Helicopter Rotors*. NASA TR R-451, 1-59, **1975**.